POST-BUCKLING INSTABILITY OF STEEL BEAM-COLUMNS

By Masayoshi Nakashima,[1] A. M. ASCE, Takeshi Nakamura,[2] and Minoru Wakabayashi,[3] M. ASCE

ABSTRACT: This paper describes an investigation of buckling and post-buckling behavior of steel beam-columns. Beam-columns having a H-shaped cross section were studied for their deformability as well as ultimate strength. A constant axial thrust and monotonically increasing end moments were applied to the beam-columns. Both experimental and analytical investigations were made in the study. Variables in the experimental study were cross-sectional shape, length, and intensity of axial force. Numerical analysis demonstrated its capability to properly simulate the behavior of the tested beam-columns. On the basis of parametric study using the numerical analysis, important findings can be drawn. First, lateral torsional deflection is more distinguished for beam-columns with less axial force. Second, beam-columns having a small slenderness ratio do not lead to instability by lateral torsional buckling, indicating a stable plastic range. Third, deformability drastically decreases once the slenderness ratio exceeds a certain level. Available formulas which estimate the ultimate strength of beam-columns, in addition, are found to be effective.

INTRODUCTION

Structural members subjected to axial thrust and bending moment in the strong axis are classified as beam-columns. The beam-column has two modes of failure. If the beam-column is stocky, it fails due to excessive bending in its strong axis. If it is slender, a buckling, called the lateral torsional buckling, occurs, and the beam-column fails by the combined effect of in-plane and lateral deformations.

Beam-columns failing in this latter mode can further be divided into two groups in accordance with their slenderness. If the beam-column is very slender, an elastic lateral torsional buckling occurs, ultimately causing failure. If the beam-columns is relatively stocky, on the other hand, it buckles first but may sustain more load or deform further without losing its load carrying capacity. Structural engineers must accurately evaluate the strength of such beam-columns in designing structures. In plastic design or earthquake resistant design, the deformability of struc-

[1]Research Engr., Building Research Inst., Ministry of Construction, Tatehara, Oho-machi, Tsukuba-gun, Ibaraki 305 Japan.

[2]Assoc. Prof., Disaster Prevention Research Inst., Kyoto Univ., Gokasho, Uji-city, Kyoto 611 Japan.

[3]Prof., Disaster Prevention Research Inst., Kyoto Univ., Gokasho, Uji-city, Kyoto 611 Japan.

Note.—Discussion open until November 1, 1983. To extend the closing date one month, a written request must be filed with the ASCE Manager of Technical and Professional Publications. The manuscript for this paper was submitted for review and possible publication on March 8, 1983. This paper is part of the Journal of Structural Engineering, Vol. 109, No. 6, June, 1983. ©ASCE, ISSN 0733-9445/83/0006-1414/$01.00. Paper No. 18068.

tural members is as important as their strength. In plastic design, this deformability is expressed in terms of the rotation capacity. Plastic hinges in beam-columns of a structural frame are required to maintain plastic moments until the frame forms a full failure mechanism. In earthquake resistant design, the deformability is expressed by the ductility. Since the strength of beam-columns is often insufficient under conditions of severe earthquake loading, the insufficient strength needs to be compensated for by these members' ductility.

Extensive research, both experimental and theoretical, has been performed on the in-plane behavior of beam-columns, providing various useful equations to predict ultimate strength (6,8). Closed form solutions are also available for computing the elastic lateral torsional buckling load of beam-columns (2). Current research, therefore, focuses on beam-columns which buckle in the inelastic range and which possess the ability to carry external forces in the post-buckling range. Van Kuren and Galambos (17) tested a number of beam-columns having a variety of geometrical shapes under various loading and support conditions. Miranda and Ojalvo (11) and Fukumoto and Galambos (4) made theoretical investigations into the inelastic lateral torsional buckling of beam-columns. They determined the buckling load using the eigenvalue analysis. The results derived by these works and others have been reduced to simple and practical equations, figures, and tables, which are summarized elsewhere (8).

One can also find works which were devoted to investigating the deformability of beam-columns. Lay (10) developed an analytical procedure to predict the rotation capacity of beams that fail ultimately either by excessive lateral deformation or by local buckling and demonstrated the capability of his procedure to properly estimate the rotation capacity resulting from experiments. Based on his study, the present American Institute of Steel Construction (AISC) specification (14) prescribes equations to compute the maximum unbraced length of beams that assures sufficient rotation capacity. This code suggests using the same equations for beam-columns. Suzuki, et al. (15,16) have carried out experimental and theoretical studies of H-shaped beam-columns subjected to constant axial force and end moments about the strong axis. They noted the rotation capacity of beam-columns in which the moment was applied at one end (with a triangular moment distribution) was more than 10 if the slenderness ratio about the weak axis was below 40; this rotation capacity rapidly decreased as the ratio increased. Beam-columns under uniform moment, on the other hand, were found to have less rotation capacity. For example, such a beam-column with a slenderness ratio of 20 had a rotation capacity of only 3.

As previously analyzed, early studies (4,11,17) directed attention to the evaluation of inelastic lateral torsional buckling load. Having been made based mainly on those studies the design formulas stipulated for strength evaluation (6,8) have not been fully calibrated for members exhibiting inelastic lateral torsional buckling. The buckling, however, may not lead the members to complete failure. Furthermore, it has not yet been verified whether or not Lay's analytical procedure to estimate rotation capacity, which originally was developed for beams, can also be applied to beam-columns. Work done by Suzuki, et al., which placed

emphasis on deformability evaluation, has provided some data. Applicability of their results, however, is limited.

Considering these uncertainties, the writers carried out a series of experiments and numerical analysis of steel H-shaped unbraced beam-columns. The study focused on: (1) Examining the true margin of additional load carrying capacity after buckling; and (2) investigating the effects of length, cross-sectional shape, and intensity of axial force of beam-columns on their rotation capacity. The beam-columns investigated in this study were simply supported in the strong axis, clamped in the weak axis, and restrained from torsional displacement and warping at both ends. In building structures ends of interior columns are connected to beams running in both horizontal directions. The beam size is usually the same in both directions, indicating rotatory restraint is considerably larger about the weak axis than about the strong axis. The support condition employed in this study is considered to be representative of this type of connection. The adopted loading condition was such that the beam-column was subjected to constant concentric axial thrust and monotonically increasing uniform moment about the strong axis. Since the study focuses on post lateral torsional buckling instability of beam-columns, flanges and webs of the beam-columns were taken to be relatively thick. To avoid premature local buckling, the width-to-thickness ratio was limited to 15 and 29 for flanges and webs, respectively. The study did not consider the effect of residual stresses on the behavior of the beam-columns.

Experimental Study

A total of 14 specimens were tested. Eight of them had a cross-sectional shape of 125 mm × 125 mm × 6.5 mm × 9 mm. These values indicate the depth of the beam-column, the flange width, the web thickness, and the flange thickness, respectively. Six of the specimens had a cross-sectional shape of 125 mm × 60 mm × 4 mm × 4 mm. The first eight specimens, designated as H-Series specimens (H-1–H-8), were taken to be representative of typical column members in a structural frame. The remaining specimens were designated as I-Series specimens (I-1–I-6), and represented column members which have a small flexural capacity in the weak axis. The geometrical and material properties of the specimens are tabulated in Tables 1, 2, and 3. To eliminate the effect of residual stresses on the characteristics of the specimens, they were annealed before testing. The length of H-Series specimens was either 1,250 mm, 2,500 mm, 3,250 mm, or 3,750 mm. The slenderness ratio, then, ranged from 24 to 71 about the strong axis and from 40 to 120 about the weak axis. I-Series specimens were 750 mm, 1,250 mm, or 2,000 mm in length. Their slenderness ratio ranged from 15 to 41 about the strong axis and from 62 to 170 about the weak axis.

Test Setup.—An overall view of the test setup is shown in Fig. 1, and the details are shown in Fig. 2. The setup was developed to ensure the support condition adopted in the study; simple support about the strong axis bending, clamped support about the weak axis bending, the torsion, and the warping. The specimen was tightened at the ends to two L-shaped arms (D in Fig. 2). Each of the arms was pin-supported at one

TABLE 1.—Geometrical Properties of H-Series Test Specimens

Entry (1)	Unit (2)	H-1 (3)	H-2 (4)	H-3 (5)	H-4 (6)	H-5 (7)	H-6 (8)	H-7 (9)	H-8 (10)
Depth	mm	125.5	124.2	124.2	124.0	124.0	124.0	126.2	125.3
	(in.)	4.933	4.893	4.893	4.886	4.886	4.886	4.972	4.937
Flange width	mm	125.1	124.8	124.9	124.9	125.0	125.0	124.8	125.4
	(in.)	4.929	4.917	4.921	4.921	4.925	4.925	4.917	4.941
Web thickness	mm	6.85	6.85	6.35	6.48	6.58	6.37	6.90	6.95
	(in.)	0.270	0.270	0.250	0.255	0.259	0.251	0.272	0.274
Flange thickness	mm	9.75	8.89	8.80	8.73	8.88	8.73	8.57	8.58
	(in.)	0.384	0.350	0.347	0.344	0.350	0.344	0.338	0.338
Cross-sectional area	mm^2	3,170	2,950	2,860	2,870	2,950	2,970	2,830	2,950
	($in.^2$)	4.91	4.57	4.43	4.45	4.57	4.60	4.39	4.57
Moment of inertia (*X*-axis)	$mm^4 \times 10^6$	8.33	8.07	7.93	7.94	7.98	7.90	8.09	8.09
	($in.^4$)	20.0	19.4	19.1	19.1	19.2	19.0	19.4	19.4
Moment of inertia (*Y*-axis)	$mm^4 \times 10^6$	3.19	2.90	2.85	2.84	2.90	2.89	2.76	2.75
	($in.^4$)	7.76	6.97	6.85	6.82	6.97	6.94	6.63	6.61
Radius of gyration (*X*-axis)	mm	52.8	52.3	52.5	52.5	52.1	52.5	52.1	52.1
	(in.)	2.08	2.06	2.07	2.07	2.05	2.07	2.05	2.05
Radius of gyration (*Y*-axis)	mm	31.7	31.2	31.5	31.4	31.4	31.7	31.2	31.4
	(in.)	1.25	1.23	1.24	1.24	1.24	1.25	1.23	1.24
Length	mm	1,248	1,250	2,506	2,500	3,252	3,250	3,751	3,750
	(in.)	49.18	49.25	98.74	98.50	128.1	128.1	147.8	147.7
Slenderness ratio (*X*-axis)		23.7	23.9	47.5	47.5	62.5	62.0	70.7	71.9
Slenderness ratio (*Y*-axis)		39.4	39.7	79.1	79.5	103.7	102.5	120.1	123.3
Axial force relative to yield force (P/P_y)		0.30	0.60	0.19	0.30	0.30	0.60	0.30	0.60

end, and a jack (B or C in Fig. 2) installed at the other end produced end moment. Axial force was applied by the jack A in Fig. 2. In order to ensure that the arms would rotate only in their own planes, apparatuses E and F were attached to the L-shaped arms. These apparatuses produced no resistance as long as the arms moved in their own planes but provided strong resistance against any out-of-plane movement of the arms. A set of round bearings and rollers (G in Fig. 2) was installed between the L-shaped arm and the head of the jack for axial force (A in Fig. 2) to minimize friction when the arm rotated. Axial force was finely adjusted with this apparatus so the force could be applied to the centroid of the specimen.

Test Procedure.—For testing, a specimen was first securely fastened to the L-shaped arms. Axial force with an intensity of approximately 10% of the yield axial force was applied to the specimen to check whether or not the force was concentric, and if necessary, fine adjustment was made by the bearing and rollers until the eccentricity was reduced to a negligible amount. Then the force was released, and measuring instruments were attached at the specimen. The instruments included load cells, dial gages to measure end rotations, LVDT's to measure lateral and vertical displacements of the midsection of the specimen, and strain gages

TABLE 2.—Geometrical Properties of I-Series Test Specimens

Entry (1)	Unit (2)	I-1 (3)	I-2 (4)	I-3 (5)	I-4 (6)	I-5 (7)	I-6 (8)
Depth	mm	124.9	124.6	125.2	124.8	124.8	124.8
	(in.)	4.917	4.906	4.929	4.913	4.913	4.913
Flange width	mm	59.5	59.8	59.7	59.8	59.7	59.6
	(in.)	2.34	2.35	2.35	2.35	2.35	2.35
Web thickness	mm	4.20	4.20	4.20	4.15	4.20	4.20
	(in.)	0.165	0.165	0.165	0.163	0.165	0.165
Flange thickness	mm	4.03	4.03	4.05	4.20	4.03	4.03
	(in.)	0.159	0.159	0.160	0.165	0.159	0.159
Cross-sectional area	mm^2	976	1,066	988	1,081	978	978
	(sq in.)	1.51	1.652	1.531	1.676	1.516	1.516
Moment of inertia (X-axis)	$mm^4 \times 10^6$	2.42	2.51	2.35	2.50	2.32	2.32
	($in.^4$)	5.81	6.03	5.65	6.01	5.57	5.57
Moment of inertia (Y-axis)	$mm^4 \times 10^6$	0.142	0.151	0.144	0.161	0.143	0.142
	($in.^4$)	0.341	0.363	0.346	0.387	0.344	0.341
Radius of gyration (X-axis)	mm	48.7	48.5	48.7	49.0	48.7	48.7
	(in.)	1.92	1.91	1.92	1.93	1.92	1.92
Radius of gyration (Y-axis)	mm	12.1	12.2	12.1	12.2	12.1	12.1
	(in.)	0.476	0.480	0.476	0.480	0.476	0.476
Length	mm	753	753	1,250	1,252	2,001	2,000
	(in.)	29.6	29.6	49.21	49.29	78.78	78.74
Slenderness ratio (X-axis)		15.4	15.5	25.9	25.4	41.1	41.1
Slenderness ratio (Y-axis)		62.1	61.4	103.6	99.6	165.5	165.8
Axial force relative to yield force (P/P_y)		0.20	0.40	0.20	0.40	0.20	0.40

TABLE 3.—Material Properties of Test Specimens

Specimen (1)	Part (2)	Yield stress (3)	Modulus of elasticity (4)	Ultimate stress (5)	Ultimate strain (6)
	Unit	MPa (kip)	GPa (kip)	MPa (kip)	m/m (in./in.)
H-Series (125 × 125 × 6.5 × 9)	Flange	243 (35.2)	205 (29.7×10^3)	384 (55.7)	0.31
	Web	269 (39.0)	187 (27.1×10^3)	410 (59.4)	0.28
I-Series (125 × 60 × 4 × 4)	Flange and web	239 (34.7)	204 (29.6×10^3)	332 (48.1)	0.36

glued on the flange surfaces. For the first step of testing, a specified axial force (20%, 30%, or 60%) of the yield axial force for H-Series specimens, and 20% or 40% of the yield axial force for (I-Series specimens) was applied (Step 1). This force held constant throughout the test. Next, end moments were slowly applied to the specimen, and stopped when a predetermined moment or rotation increment was attained (Step 2). The

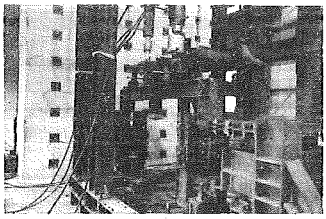

FIG. 1.—Overall View of Test Setup

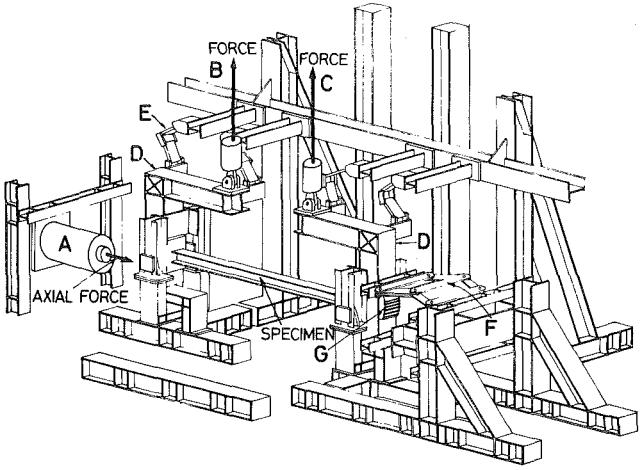

FIG. 2.—Details of Test Setup

axial force was checked again and adjusted to the specified level when necessary (Step 3). All the instruments were read after they stopped fluctuating (Step 4). Steps 2–4 were repeated until one of the following conditions occurred: (1) The axial force could not maintain its level due to excessive damage; (2) the end moments were reduced to zero; or (3) the loading jacks exhausted their strokes.

Test Results.—Figures 3 and 4 show the end moment (M) vs. the end rotation (θ) curves of the test specimens. The moment and rotation are nondimensionalized by the plastic moment (M_p) and the yield end rotation (θ_p), respectively. Symbols, *CR* and *LB*, in the figures, denote the points of lateral torsional buckling and of local buckling. Table 4 tabulates the ultimate moment (M_u), the lateral torsional buckling moment (M_{cr}), and the rotation capacity (R). The rotation capacity was calculated as

$$R = \frac{\theta_u}{\theta_p} - 1 \quad \ldots\ldots (1)$$

θ_u was taken as the rotation at which the moment was reduced to 95% of the ultimate moment in the unstable (negative slope) range.

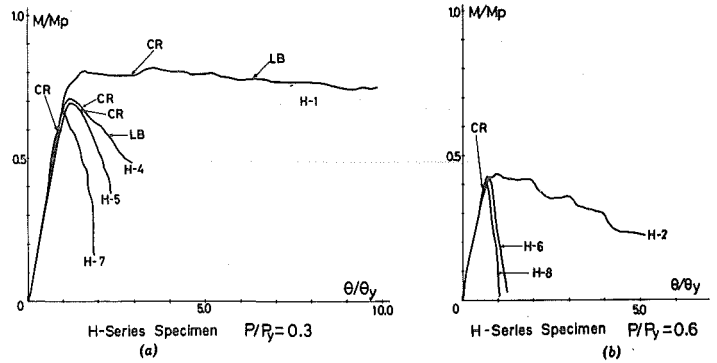

FIG. 3.—Moment versus Rotation Curves of H-Series Specimens

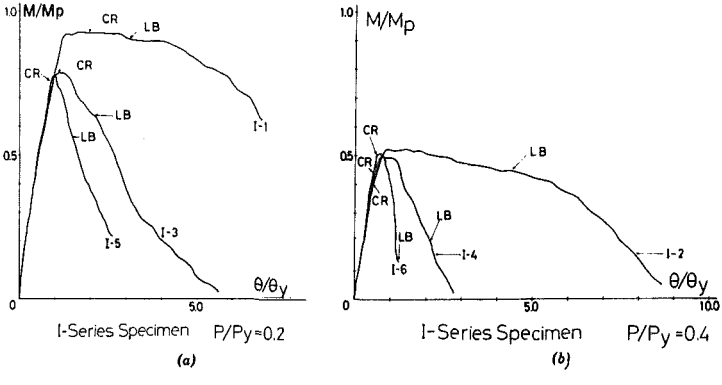

FIG. 4.—Moment versus Rotation Curves of I-Series Specimens

In H-Series specimens, lateral deformation was not accelerated after lateral torsional buckling was initiated. The lateral deformation was most significant in Specimen H-1, which was most stocky and subjected to the smallest axial force. This specimen, nevertheless, exhibited high performance in rotation capacity [Fig. 3(*a*)]. Other specimens failed primarily because of excessive in-plane bending with minimal lateral deformation observed. It was found that strength and deformation of the specimens were influenced slightly by the lateral torsional buckling. Lateral deformation of I-Series specimens increased rapidly once they buckled, and that deformation apparently reduced the rotation capacity of the specimens.

Local buckling, observed at compression flanges near the ends and mid-span, took place when the moment decreased significantly after the ultimate moment was passed, except for Specimens H-1 and I-1. In these specimens (H-1 and I-1), the local buckling occurred shortly after the ultimate moment. However, the buckling does not accelerate the reduction in moment as shown in Figs. 3(*a*) and 4(*a*). Local buckling was found to have, at most, a secondary effect on the post-buckling instability of the test specimens.

TABLE 4.—Ultimate Moment, Buckling Moment, and Rotation Capacity of Test Specimens

Specimen (1)	Maximum Moment (M_u/M_p) (2)	Lateral Torsional Buckling Moment (M_{cr}/M_p) (3)	Rotation Capacity (R) (4)
H-1	0.812	+0.788	4.68
H-2	0.434	No buckling	2.15
H-3	0.917	−0.913	1.47
H-4	0.691	+0.677	0.396
H-5	0.681	+0.651	0.238
H-6	0.425	No buckling	0.010
H-7	0.669	−0.589	0.005
H-8	0.403	−0.376	0.001
I-1	0.923	−0.910	2.19
I-2	0.518	−0.405	1.83
I-3	0.798	−0.798	0.340
I-4	0.500	−0.456	0.910
I-5	0.778	−0.757	0.320
I-6	0.498	−0.447	0.415

Note: Symbols + and − indicate that the buckling occurred after and before the maximum moment was attained.

Numerical Analysis

The eigenvalue analysis can predict the lateral torsional buckling of beam-columns. If the concept of the tangent modulus or of the reduced modulus is employed, the analysis can be extended to compute the critical load of beam-columns that buckle in their inelastic range (4,11). However, with the tangent modulus concept, the eigenvalue analysis assesses the lower limit of the buckling load at most. The ultimate load of a beam-column could be greater than its buckling load while the margin of additional strength changes corresponding to the geometry and loading and support conditions of the beam-column. Neither does the analysis give any indication of the deformation after buckling. The inelastic post-buckling behavior of a beam-column is best analyzed by considering the equilibriums of the beam-column after it buckles. The analysis, therefore, is essentially the same as that of a beam-column subjected to biaxial bending.

Birnstiel and Michalos (1), Harstead, et al. (9), Sharma and Gaylord (13), Santathadaporn and Chen (12), and Fujimoto and Matsumoto (3) have developed numerical models for the analysis of H-shaped beam-columns subjected to biaxial bending. In their studies, flexural, torsional, and warping stiffnesses of a beam-column were computed by taking into account possible penetration of plastic flow in its cross section. The governing equilibrium equations were solved by either assuming deflected shapes or employing the finite difference method. In the writers' study, a beam-column was analyzed by assuming that it has a small crookness about the weak axis. With this assumption, lateral as well as in-plane instability can be examined because equilibriums about

the weak axis and the torsion, in addition to the equilibrium about the strong axis, are taken into account.

Procedure of Analysis.—Several basic assumptions were employed in the analysis. First, the stress vs. strain relationship of the steel was taken to be bilinear (with E and αE as the moduli) as shown in Fig. 5. The strain reversal was taken into account, with the modulus in the unloading branch being identical with the elastic modulus (E). Second, it was assumed the cross-sectional shape of the beam-column did not change during loading. That is, the flanges and web would not deform in out-of-plane directions. Through this assumption, displacements of any point in the flanges or web can uniquely be related to the centroidal displacements of the cross section. Third, the residual stresses were not included in the analysis.

As computation involved iterative operations because of the inelastic behavior of the beam-columns, the governing equations were expressed in an incremental form. Thus

$$\overline{EI}_x \times \Delta v_s'' + \Delta M + P \times (\Delta v_s + x_s \times \Delta\phi) = 0 \quad \ldots\ldots (2)$$

$$\overline{EI}_y \times \Delta u_s'' + M \times \Delta\phi + \Delta M \times \phi + P \times (\Delta u_s + y_s \times \Delta\phi) = 0 \quad \ldots\ldots (3)$$

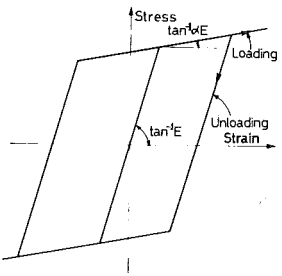

FIG. 5.—Stress versus Strain Relationship Used in Analysis

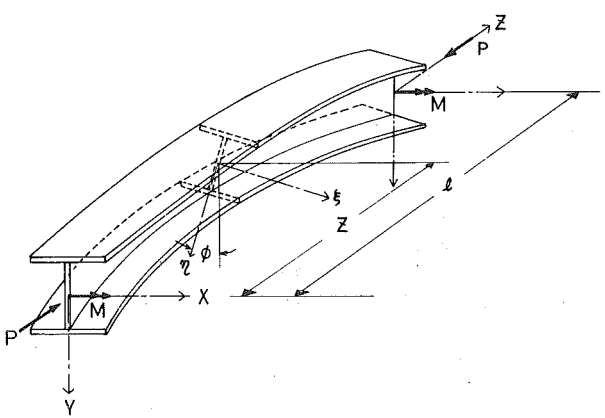

FIG. 6.—Coordinate System Used in Analysis

$$\overline{EI}_w \times \Delta\phi''' - (\overline{GK}_t + \overline{K}) \times \Delta\phi' + \Delta M \times u_s' + M \times \Delta u_s'$$
$$+ P \times y_s \times \Delta u_s' - P \times x_s \times \Delta v_s' = 0 \quad \ldots\ldots (4)$$

Equations 2–4 represent, respectively, the equilibriums of the strong axis (x) bending, the weak axis (y) bending, and the longitudinal axis (z) torsion. $\overline{EI}_x$, $\overline{EI}_y$, $\overline{EI}_w$, and $\overline{GK}_t$ are the flexural stiffnesses about the x and y axes, the warping stiffness, and the St. Venant torsional stiffness. Symbols, u, v, and ϕ indicate the displacements in the x and y axes and rotation of the centroid of the cross section. In addition, ξ and η constitute local coordinates as shown in Fig. 6. A set of x_s and y_s denotes the coordinates of the shear center with respect to the local coordinate system, while u_s and v_s are the displacements of the shear center with respect to the global (x-y) coordinate system. P and M are the axial force and end moment about the strong axis. Figures 6 and 7 demonstrate these terms and their sign convention; arrows indicate the positive direction. Symbol Δ denotes the increment of terms from one step to the next; for example Step n to Step $n + 1$ in Fig. 7. The stiffnesses, $\overline{EI}_x$, $\overline{EI}_y$, $\overline{EI}_w$, and $\overline{GK}_t$ are not constant once part of the stress in steel departs from the elastic range. To effectively evaluate these stiffnesses in the inelastic range, the cross section was divided into a number of small segments as shown in Fig. 8. The stress state in each segment was represented by the stress of its centroid. The flexural stiffnesses $\overline{EI}_x$ and $\overline{EI}_y$ can be written as

$$\overline{EI}_x = \Sigma\{[YF(i,j) - y_c]^2 \times EF(i,j) \times AF(i,j)\}$$
$$+ \Sigma\{[YW(i,j) - y_c]^2 \times EW(i,j) \times AW(i,j)\} \quad \ldots\ldots (5)$$

$$\overline{EI}_y = \Sigma\{[XF(i,j) - x_c]^2 \times EF(i,j) \times AF(i,j)\}$$
$$+ \Sigma\{[XW(i,j) - x_c]^2 \times EW(i,j) \times AW(i,j)\} \quad \ldots\ldots (6)$$

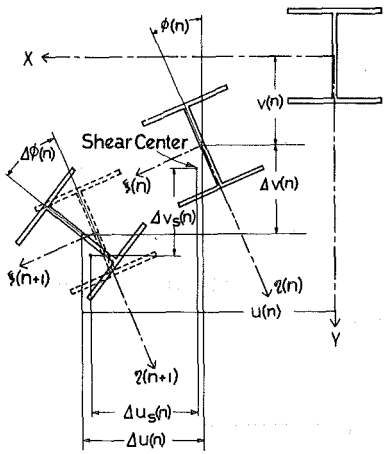

FIG. 7.—Deflected Shape of Cross Section and Its Local Coordinate System

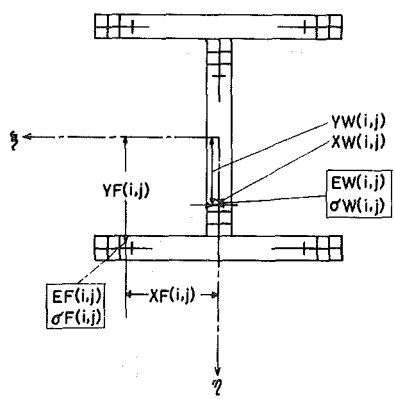

FIG. 8.—Segmentation of Cross Section

$$x_c = \frac{\Sigma[XF(i,j) \times EF(i,j) \times AF(i,j)] + \Sigma[XW(i,j) \times EW(i,j) \times AW(i,j)]}{\Sigma[EF(i,j) \times AF(i,j)] + \Sigma[EW(i,j) \times AW(i,j)]} \quad \ldots\ldots (7)$$

$$y_c = \frac{\Sigma[YF(i,j) \times EF(i,j) \times AF(i,j)] + \Sigma[YW(i,j) \times EW(i,j) \times AW(i,j)]}{\Sigma[EF(i,j) \times AF(i,j)] + \Sigma[EW(i,j) \times AW(i,j)]} \quad \ldots\ldots (8)$$

in which $XF(i,j)$ and $YF(i,j)$ = the coordinates of (i,j) segment of the flanges with respect to the local coordinate system; and $AF(i,j)$ and $EF(i,j)$ = the cross-sectional area and the modulus, either E or αE, of the segment. Similarly, $XW(i,j)$, $YW(i,j)$, $AW(i,j)$, and $EW(i,j)$ are those belonging to (i,j) segment of the web. The warping stiffness $\overline{EI}_w$ is expressed as

$$\overline{EI}_w = \Sigma\{[XF(i,j) - x_s]^2 \times [YF(i,j) - y_s]^2 \times EF(i,j) \times AF(i,j)\}$$
$$- \Sigma\{[XW(i,j) - x_s]^2 \times [YW(i,j) - y_s]^2 \times EW(i,j) \times AW(i,j)\} \quad \ldots\ldots (9)$$

$$x_s = \{\Sigma[(XF(i,j) - x_c) \times (YF(i,j) - y_c)^2 \times EF(i,j) \times AF(i,j)]$$
$$+ \Sigma[(XW(i,j) - x_c) \times (YW(i,j) - y_c)^2 \times EW(i,j) \times AW(i,j)]\} \div \overline{EI}_x \quad \ldots\ldots (10)$$

$$y_s = \{\Sigma[(XF(i,j) - x_c)^2 \times (YF(i,j) - y_c) \times EF(i,j) \times AF(i,j)]$$
$$+ \Sigma[(XW(i,j) - x_c)^2 \times (YW(i,j) - y_c) \times EW(i,j) \times AW(i,j)]\} \div \overline{EI}_y \quad \ldots\ldots (11)$$

The terms x_c and y_c, and x_s and y_s, in the preceding equations have a physical meaning that they are the coordinates of the center of gravity and of the shear center of the cross section with possible yielding of part of the section considered. The St. Venant torsional stiffness $\overline{GK}_t$ is taken to be

$$\overline{GK}_t = G \times K_t \times \left(\frac{A_{\text{red}}}{A}\right) \quad \ldots\ldots (12)$$

$$A_{\text{red}} = \Sigma\left[AF(i,j) \times \frac{EF(i,j)}{E}\right] + \Sigma\left[AW(i,j) \times \frac{EW(i,j)}{E}\right] \quad \ldots\ldots (13)$$

The previous equation is made with the assumption the shear modulus of yielded segments be reduced to αG with G as the shear modulus. The term $\overline{K}$ in Eq. 4 reflects the torsional restraint caused by the steel fibers' inclination about the z axis. This term is explained in detail.

$$\overline{K} = \Sigma[\sigma F(i,j) \times (XW(i,j) - x_s)^2 \times (YF(i,j) - y_s)^2 \times AF(i,j)]$$
$$+ \Sigma[\sigma W(i,j) \times (XW(i,j) - x_s)^2 \times (YW(i,j) - y_s)^2 \times AW(i,j)] \quad \ldots\ldots (14)$$

To solve the governing equations (Eqs. 2–4), deflected shapes of the beam-column were assumed as

$$\Delta v_s = \sum_{i=1}^{i=k} \left\{DV_s(i) \times \sin\left[(2i-1) \times \pi \times \frac{z}{l}\right]\right\} \quad \ldots\ldots (15)$$

$$\Delta u_s = \sum_{i=1}^{i=k} \left\{DU_s(i) \times \left[\cos\left(2i \times \pi \times \frac{z}{l}\right) - 1\right]\right\} \quad \ldots\ldots (16)$$

$$\Delta\phi = \sum_{i=1}^{i=k} \left\{ D\phi(i) \times \left[\cos\left(2i \times \pi \times \frac{z}{l}\right) - 1 \right] \right\} \quad \ldots\ldots (17)$$

in which $Dv_s(i)$, $Du_s(i)$, and $D\phi(i)$ = the constants to be solved; and l = the length of the beam-column. The deflected shapes satisfy the support conditions used in the experiment. At each incremental step, the equations were first solved by taking the stiffnesses in the previous step and then correcting them in accordance with the strain state of the cross section. Derived displacement increments of the shear center, Δu_s and Δv_s, were converted to centroidal displacement increments by the equations

$$\Delta u(n) = \Delta u_s(n) + y_s(n) \times \Delta\phi(n) \quad \ldots\ldots (18)$$

$$\Delta v(n) = \Delta v_s(n) - x_s(n) \times \Delta\phi(n) \quad \ldots\ldots (19)$$

The total displacements of the centroid, therefore, were given by

$$u(n) = \sum_{m=1}^{m=n} \Delta u(m) \quad \ldots\ldots (20)$$

$$v(n) = \sum_{m=1}^{m=n} \Delta v(m) \quad \ldots\ldots (21)$$

$$\phi(n) = \sum_{m=1}^{m=n} \Delta\phi(m) \quad \ldots\ldots (22)$$

Examples.—In order to assess the capacity of this numerical model, tested specimens were analyzed by using the model. Figure 9 shows the midspan displacements and rotation of Specimens H-1 and I-5. Solid lines denote the displacements and rotation obtained by the test, whereas dashed lines show those derived from the analysis. The elastic modulus, yield stress, and geometrical properties tabulated in Tables 1–3 were employed in the analysis. In addition, the modulus in the second branch (αE) was taken to be 1/300 of the elastic modulus, and as an initial

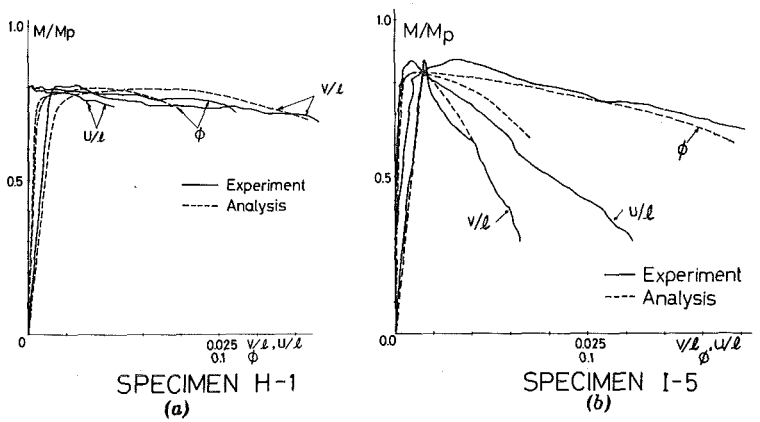

FIG. 9.—Comparison of Experimental and Analytical Moment versus Deflection Curves

crookness in the weak axis, a full wave of the cosine curve was used with an amplitude of 1/500 of the column length (l). As demonstrated in Fig. 9, correlation between the experiment and analysis is satisfactory.

Analysis

Ultimate Strength of Beam-Columns.—To estimate the ultimate moment of a beam-column subjected to axial force and uniform moment, the present AISC Specification (14) prescribes

$$\frac{P}{P_{cr}} + \frac{M}{\left(\frac{1-P}{P_e}\right) \times M_m} \leq 1.0 \quad \ldots\ldots (23)$$

in which: P_e = Euler buckling force; and M_m = maximum moment that can be resisted by the member in the absence of axial force. Further, $M_m = M_p$ if the beam-column is braced in the weak direction. If it is not

$$M_m = \left[1.07 - \frac{\lambda_y \times \sqrt{F_y}}{3{,}160}\right] \times M_p \leq M_p \quad \ldots\ldots (24)$$

The numerical analysis was made with a variety of lengths and axial force levels for beam-columns having the cross section used in H- or I-Series tests, and the results were compared with Eq. 23. Two of the relationships between the ultimate moment and the slenderness ratio about the strong axis (λ_x) are shown in Fig. 10. In this figure, the dashed line was developed from Eq. 23 with $M_m = M_p$; meanwhile the chain line was from Eq. 23 with Eq. 24, and the solid line from the analysis, while the experimental results are plotted as black squares. From this analysis, several conclusions can be drawn. Beam-columns having the cross section used in H-Series tests (H-shaped beam-columns) are capable of resisting at least as much moment as that prescribed in Eq. 23 combined with Eq. 24. This conclusion indicates the reduction in strength due to lateral deformation is minimal. Therefore, the combination of Eqs. 23 and 24 appears to lead to an overconservative design. On the other hand, the lateral deformation apparently affects the ultimate moment of

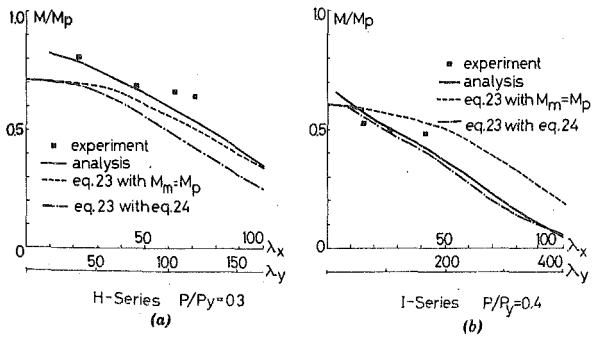

FIG. 10.—Interaction Curves between Slenderness Ratio and End Moment

beam-columns having the cross section used in I-Series tests (I-shaped beam-columns) as was partially verified in the tests. Thus, the combination of Eqs. 23 and 24 is found to effectively predict the ultimate moment.

Rotation Capacity.—In the present study, variables that affect the rotation capacity are: (1) Intensity of axial force; (2) the slenderness ratio about the strong axis; and (3) the slenderness ratio about the weak axis. The influence of these variables on the rotation capacity and their interaction are analyzed in this section.

Both U.S. and Japanese specifications (14,7) specify a maximum allowable slenderness ratio about the weak axis to ensure sufficient rotation capacity.

They are:

$$\frac{lcr}{r_y} \leq \frac{1{,}375}{F_y} \quad \text{(AISC Specification, Eq. 2.9-1}b\text{)} \ldots\ldots\ldots\ldots\ldots\ldots \quad (25)$$

$$\frac{lh}{A_f} \leq 250 \quad \text{and} \quad \frac{l}{r_y} \leq 65$$

[Japanese Plastic Design Guide, Eq. 5-18(a)] $\ldots\ldots\ldots\ldots\ldots\ldots$ (26)

Equation 25 is stipulated on the basis of the work done by Lay (10). In this equation, sufficient rotation capacity is taken to be from about 8 to 10 in accordance with the material properties of steel. Equation 26, on the other hand, was empirically derived on the basis of the results of beam tests carried out in Japan. Sufficient rotation capacity is not defined clearly in the equation but is implicity taken to be in the range of 2 to 4. In these equations, the effect of axial force is not included directly. The AISC specification suggests the use of Eq. 25 for both beams and beam-columns. Figure 11 shows relationship between slenderness ratio and rotation capacity of beam-columns having a cross section used in H- and I-Series tests. Curves in the figure were obtained by means of the numerical analysis. Equation 25 effectively predicts the rotation capacity of the H-shaped beam-columns except for the one with P/P_y = 0.6, while Eq. 26 roughly indicates the point at which the curves begin to increase precipitously. Both Eqs. 25 and 26 give a significantly con-

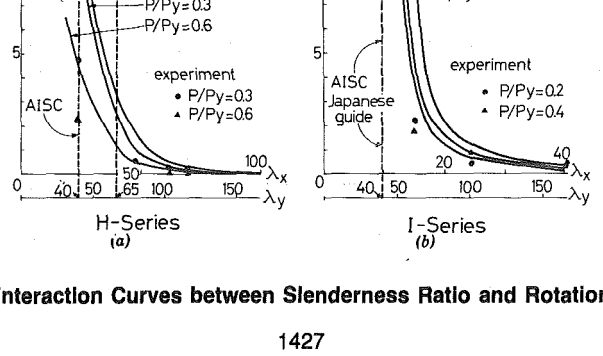

FIG. 11.—Interaction Curves between Slenderness Ratio and Rotation Capacity

servative result for I-shaped beam-columns.

The definition of a sufficient rotation capacity is debatable. In a highly indeterminate structure, some hinges must rotate a great deal before reaching a mechanism. Whereas the last hinge before the mechanism, however, does not need to have any rotation capacity. Nevertheless, since various loading patterns should be considered in designing structures, it seems reasonable to require critical components of structures, like columns in the first story, to possess a rotation capacity of more than five. Therefore, Eq. 25 is adequate enough to assure sufficient rotation capacity of beam-columns.

The question remains whether or not the effect of axial force on rotation capacity should be incorporated explicitly into the equation. The curve with $P/P_y = 0.6$ [Fig. 11(*a*)] intersects the value indicated by Eq. 25 at a rotation capacity of 4.5, which may not be considered sufficient. Nevertheless, the writers support the use of the equation for the following reasons in addition to its simplicity. The axial force varies during loading because occurrence of new hinges changes the internal force distribution. External forces that may vary with time also changes the level of axial forces. As a result, it is impractical to expect beam-columns to hold the axial force constant. In addition, since high axial force tends to enhance lateral deflection caused by the P-Δ effect, it is more reasonable to set an upper limit of allowable axial force; for example 30% of the yield axial force. With this limitation, a rotation capacity of 10 can be assured for H-shaped beam-columns [Fig. 11(*a*)].

As indicated in Fig. 11(*b*), Eq. 25 gives a conservative estimate for the I-shaped beam-columns. The ratio of slenderness about the weak axis to slenderness about the strong axis is greater for I-shaped beam-columns than for H-shaped beam-columns. This means that if the slenderness about the weak axis is identical between the two types of beam-columns, I-shaped beam-columns are more stocky about the strong axis, and accordingly have better rotation capacity. Since Eq. 25 gives a good prediction for H-shaped beam-columns [Fig. 11(*a*)], the requirement of allowable unsupported length (to ensure sufficient rotation capacity) may be liberalized according to the ratio of slenderness about the two axes. Further research is needed to investigate the effect of the relative slenderness about the two axes on rotation capacity and to propose a liberalized requirement if this is found reasonable.

Conclusion

Buckling and post-buckling behavior of steel beam-columns having H-shaped cross sections were examined by experiments and numerical analysis. Important findings and areas of further research can be summarized as follows.

For beam-columns having wide flanges (H-shaped beam-columns), the effect of lateral torsional buckling on their ultimate strength (moment) is minimal, and their strength can be predicted on the basis of their in-plane behavior. For beam-columns having narrow flanges (I-shaped beam-columns) Eq. 2.4-2 of the AISC specification is adequate in estimating their ultimate strength.

Equation 2.9-1 of the AISC specification is useful to ensure a rotation

capacity of about 10 for H-shaped beam-columns. The axial force, however, should not exceed 30% of the yield axial force in the design of these beam-columns. Equation 2.9-1 (14) provides a significantly conservative estimation of unsupported length of I-shaped beam-columns. Additional study is underway to investigate the effect of relative slenderness about the two axes on rotation capacity, aiming at possible liberalization of the unsupported length requirement for beam-columns with narrow flanges. Influences of residual stresses, moment gradient, lateral force, and support conditions on rotation capacity are also subjects that require further study.

Appendix I.—References

1. Birnstiel, C., and Michalos, J., "Ultimate Load of H-Columns under Biaxial Moment," *Journal of the Structural Division*, ASCE, Vol. 89, No. ST2, Apr., 1963, pp. 161–197.
2. Bleich, F., *The Buckling Strength of Metal Structures*, McGraw-Hill Book Co., Inc., New York, N.Y., 1952.
3. Fujimoto, M., and Matsumoto, Y., "Study on the Inelastic Behavior of Columns of H-Shaped Cross Section under Biaxial Bending, Part 1 and 2," *Transactions of Architectural Institute of Japan*, No. 173, July, 1970, pp. 37–47 (in Japanese).
4. Fukumoto, Y., and Galambos, T. V., "Inelastic Lateral-Torsional Buckling of Beam-columns," *Journal of the Structural Division*, ASCE, Vol. 93, No. ST2, Apr., 1966, pp. 41–61.
5. Galambos, T. V., *Structural Members and Frames*, Prentice Hall Inc., Englewood Cliffs, N.J., 1968.
6. "Guide to Buckling Design of Steel Structures," Gihodo Inc., Architectural Institute of Japan, Tokyo, Japan, 1980 (in Japanese).
7. "Guide to Plastic Design for Steel Structures," Gihodo Inc., Architectural Institute of Japan, Tokyo, Japan, 1976 (in Japanese).
8. "Guide to Stability Design Criteria for Metal Structures," Structural Stability Research Council, 3rd ed., Wiley Interscience, New York, N.Y., 1976.
9. Harstead, G. A., Birnstiel, C., and Leu, K. C., "Inelastic H-Columns under Biaxial Bending," *Journal of the Structural Division*, ASCE, Vol. 94, No. ST10, Oct., 1968, pp. 2371–2398.
10. Lay, M. G., "The Static Load-Deformation Behavior of Plannar Steel Structure," dissertation presented to the Department of Civil Engineering , at Lehigh University, in Bethlehem, Pa., in 1964, in partial fulfillment of the requirement for the degree of Doctor of Philosophy.
11. Miranda, D., and Ojalvo, M., "Inelastic Lateral-Torsional Buckling of Beam Columns," *Journal of the Engineering Mechanics Division*, ASCE, Vol. 92, No. EM6, Dec., 1965, pp. 21–37.
12. Santathadaporn, S., and Chen, W. F., "Tangent Stiffness Method for Biaxial Bending," *Journal of the Structural Division*, ASCE, Vol. 98, No. ST1, 1972, pp. 153–163.
13. Sharma, S. S., and Gaylord, E. H., "Strength of Steel Columns With Biaxially Eccentric Load," *Journal of the Structural Division*, ASCE, Vol. 95, No. ST12, Dec., 1969, pp. 2797–2812.
14. "Specification for the Design, Fabrication and Erection of Structural Steel for Buildings," American Institute of Steel Construction, New York, N.Y., 1978.
15. Suzuki, T., and Ono, T., "Experimental Study of Bracing Beam-Columns," *Transactions of Architectural Institute of Japan*, No. 188, Oct., 1971, pp. 33–40 (in Japanese).
16. Suzuki, T., Ono, T., and Kato, M., "Rotation Capacity of H-Shaped Beam-Columns, Part 1 and 2," *Annual Transactions of Architectural Institute of Japan*, Oct., 1976, pp. 1009–1012 (in Japanese).
17. Van Kuren, R. D., and Galambos, T. V., "Beam Column Experiments," *Jour-*

nal of the Structural Division, ASCE, Vol. 90, No. ST2, Apr., 1963, pp. 223–256.

APPENDIX II.—NOTATION

The following symbols are used in this paper:

A = cross-sectional area of a beam-column;
$AF(i,j), AW(i,j)$ = areas of flange and web (i,j) segments;
A_f = cross-sectional area of a flange;
A_{red} = effective cross-sectional area of a beam-column;
$DU_s(i), DV_s(i), D\phi(i)$ = coefficients to be solved;
$EF(i,j), EW(i,j)$ = modului of flange and web (i,j) segments;
$\overline{EI}_w$ = warping stiffness;
$\overline{EI}_x, \overline{EI}_y$ = flexural stiffnesses about x and y axes;
F_y = specified minimum yield stress, in kips per square inch, if used with the radical sign;
G = shear modulus;
$\overline{GK}_t$ = St. Venant torsional stiffness;
h = depth of a beam-column measured about the strong axis;
l = length of a beam-column;
M = end moment;
M_{cr} = lateral torsional buckling moment;
M_m = critical moment that can be resisted by a plastically designed member in the absence of axial load;
M_p = plastic moment;
M_u = ultimate moment;
P = axial force;
P_{cr} = maximum strength of an axially loaded compression member;
P_e = Euler buckling load;
P_y = yield axial force;
R = rotation capacity;
r_x, r_y = radii of gyration about x and y axes;
$\langle u, v, \phi \rangle$ = centroidal displacements and rotation;
$\langle u_s, v_s \rangle$ = displacements of shear center;
$\langle XF(i,j), YF(i,j) \rangle$ = coordinates of flange (i,j) segment;
$\langle XW(i,j), YW(i,j) \rangle$ = coordinates of web (i,j) segment;
$\langle x, y, z \rangle$ = global coordinate system;
$\langle x_c, y_c \rangle$ = coordinates of effective center of gravity;
$\langle x_s, y_s \rangle$ = coordinates of shear center;
α = ratio of strain hardening modulus to elastic modulus;
Δ = prefix to represent increment;
θ = end rotation;
θ_p = yield end rotation;
θ_u = ultimate end rotation;
λ_x, λ_y = slenderness ratio about x and y axis;
$\langle \xi, \eta \rangle$ = local coordinate system; and
$\sigma F(i,j), \sigma W(i,j)$ = stresses of flange and web (i,j) segments.